Microstructure and nanomechanical properties of nitrogenated amorphous carbon thin films synthesized by reactive RF sputtering

W. Lu and K. Komvopoulos
Department of Mechanical Engineering, University of California, Berkeley, California 94720

Abstract

Thin films of nitrogenated amorphous carbon (a-CN_x) were deposited on Si(100) substrates by reactive RF sputtering using a gas mixture of Ar and N_2 at a total working pressure of 3 mTorr. X-ray photoelectron spectroscopy (XPS) revealed that the films consisted of amorphous carbon (a-C) containing a β-C_3N_4-like phase with N atoms bonded to C atoms in tetrahedral coordination (sp^3) and a graphite-like phase with N atoms bonded to C atoms in trigonal coordination (sp^2). Analysis of the XPS spectra showed a strong effect of the N_2 partial pressure on the concentration and composition of each constituent. The thickness and nanohardness of the a-CN_x films were in the ranges of 10-35 nm and 11.5-43.2 GPa, respectively, depending on the amount of N_2 in the sputtering gas. Conversely to the chemical composition, the growth rate (thickness), microstructure, and nanomechanical properties of the a-CN_x films depended on the total mass flow rate. While the N/C atomic ratio increased with the N_2 partial pressure, the film nanohardness and in-plane elastic modulus decreased due to the reduced energetic ion bombardment on the growing film surface and the incorporation of soft phases in the sputtered films. Nanoindentation and XPS results are presented to elucidate the deposition kinetics and interpret the dependence of the resulting film microstructure and nanomechanical properties on the plasma conditions.

Submitted to the *Journal of Applied Physics* on June 15, 1998; revised manuscript submitted on October 20, 1998.

I. INTRODUCTION

Ultra-thin, smooth films with high hardness and toughness are of both scientific and practical significance. For example, sputtered films of hard amorphous carbon (a-C), diamond-like carbon, and nitrogenated carbon (CN_x) exhibiting low friction and high wear resistance play a critical role in magnetic recording, especially in view of current technology trends toward proximity recording to satisfy the increasing demand for higher storage densities. Because of the extremely small flying height in high-density magnetic recording, intermittent contact of the head on the rigid disk surface leads to premature failure of the disk drive in the absence of a smooth wear-resistant carbon overcoat. The notion that the mechanical properties of ***b***-C_3N_4 are similar to those of diamond[1,2] has recently generated significant interest in the development of hard CN_x films, principally to satisfy stringent surface durability requirements, such as those in proximity recording.

Among various vapor phase deposition techniques, reactive sputtering,[3-10] including DC sputtering and capacitively or inductively coupled RF sputtering (with or without magnetron confinement), nitrogen ion implantation of carbon films,[11-13] laser ablation of carbon in a nitrogen environment,[14,15] ionic nitrogen beam irradiation,[16] and ion beam deposition[3,17,18] are common methods used to synthesize CN_x films. Other less frequently used techniques include shield arc ion plating[19] and chemical vapor deposition combined with an electron cyclotron resonance plasma method.[20] The CN_x films obtained in previous studies were usually amorphous with a global N/C atomic ratio up to 0.9. Although convincing evidence for the development of ultra-hard ***b***-C_3N_4 films was not obtained, the high hardness and good tribological properties of some a-CN_x films deposited under certain conditions suggested a strong effect of process parameters on the resulting microstructure and mechanical properties of the sputtered films.

Recent studies of Marton et al.[3] and Sjostrom et al.[5] dealing with the microstructure of CN_x films have indicated the presence of a phase exhibiting a stoichiometry similar to that of ***b***-C_3N_4 with N atoms bonded to C atoms in tetrahedral coordination (sp^3) and a graphite-like phase with N atoms bonded to C atoms in trigonal coordination (sp^2). These two phases can be distinguished by their characteristic binding energies of core level electrons of C and N atoms. Thus, the composition of CN_x films cannot be simply assessed based on the overall nitrogen content; it is essential to determine the amounts of nitrogen and carbon in each constituent phase. It has been proposed that the high hardness and large elastic recovery of CN_x films are due to buckling of graphitic basal planes, resulting in a dense three-dimensional covalently-bonded network, where sp^2-bonded basal planes terminated by N atoms are bonded to sp^3-hybridized C atoms.[4,5,21] These studies may provide explanation for the high hardness and significant elastic recovery observed for some carbon films, despite their relatively large fractions of sp^2 bonding.

Although the effect of deposition conditions on the composition, microstructure, and mechanical properties of sputtered films has been considered in several previous studies, the role of plasma parameters and film growth kinetics on the properties of sputtered CN_x films has not been fully elucidated.[4,9,10] Kaltofen et al.[10] studied the plasma generated at the substrate surface during reactive RF magnetron sputtering of CN_x films in a pure nitrogen plasma, and reported that both the power density due to ion bombardment on the substrate surface and the kinetic energy per condensing C or N atom are important process parameters. It is apparent, therefore, that the actual plasma parameters in the deposition environment affect the microstructure and properties of the film. Knowledge of the film growth kinetics at different plasma conditions (or process parameters) is essential to explain the dependence of the film composition, microstructure, and mechanical properties on controlling process parameters.

In this investigation, ultra-thin films of nitrogenated amorphous carbon (a-CN_x) were deposited on smooth Si(100) substrates at about room temperature by RF reactive sputtering using a pure graphite target and a sputtering gas mixture of Ar and N_2. The volume fraction of N_2 in the sputtering gas was varied, whereas the geometrical configuration, RF power, substrate bias, and total working pressure, were set according to the optimum deposition conditions determined in previous studies dealing with the nanomechanical and nanotribological properties of nitrogen-free a-C films.[22] X-ray photoelectron spectroscopy was used to determine the compositions and binding energies of core level electrons revealing the chemical bonding states of C and N in the sputtered a-CN_x films. Surface roughness, nanoindentation hardness, and elastic modulus measurements were obtained with a surface force microprobe apparatus interfaced with an atomic force microscope. The main objectives of this study were the analysis of the film deposition kinetics and the identification of the effect of plasma conditions on the resulting microstructure and nanomechanical properties of RF sputtered a-CN_x films.

II. EXPERIMENTAL PROCEDURES

A. Reactive RF sputtering

Thin carbon films were deposited on Si(100) substrates possessing a root-mean-square (rms) roughness of ~0.2 nm by reactive RF sputtering using a modified Perkin-Elmer Randex-2400 model sputtering system. Carbon material was sputtered from a 20-cm-diameter graphite target fixed at a distance of ~7 cm above the specimen holder, which was maintained close to room temperature by water cooling. Before deposition, the graphite target was sputter cleaned in an Ar plasma for 5 min at a pressure of 3 mTorr and RF power of 250 W. Under these processing conditions, the resulting self-biased target voltage is about -900 V. The silicon substrate surface was then exposed to an Ar plasma for 3 min at a pressure of 3 mTorr, RF power of 250 W, and resulting substrate bias voltage of about -820 V to sputter etch a ~45-nm-thick surface layer. Film

deposition was then performed for 5 min at RF power of 750 W, substrate bias voltage of -200 V, and total pressure of 3 mTorr using a gas mixture of Ar and N_2. Previous work with a working gas consisting of pure Ar has demonstrated that the above optimum sputter deposition conditions produce hydrogen-free a-C films with hardness of ~40 GPa.[22] At a chamber pressure of 3 mTorr, the mean free paths of Ar and N_2 in their parent gas are equal to about 1.4 cm and 1.2 cm, respectively.[23] The base pressure in the deposition chamber was less than 5×10^{-6} Torr. To obtain molar (volume) percentages of N_2 between zero and 90%, the partial pressure of N_2 was varied between zero and 2.7 mTorr by adjusting the mass flow rates of the Ar and N_2 gasses independently, while maintaining the total working pressure fixed at 3 mTorr.

To determine the significance of the N_2 and Ar gas flow rates, carbon film deposition was performed for (a) nitrogen content and total gas flow rate ranges of 0-86 vol% and 8-13 sccm, respectively, (b) nitrogen content range of 0-80 vol% and total gas flow rate fixed at 20 sccm, and (c) nitrogen content range of 0-4 vol% and total gas flow rate fixed at 10 sccm. The deposition conditions of representative samples from the first and second sets of experiments are given in Table I (samples A-D and E-J, respectively). Only composition results from five representative samples of the third set of experiments are presented here.

Plasma heating of the specimen surface due to particle bombardment was insignificant due to the short deposition time (5 min) in a weakly ionized discharge and the water cooling of the substrate holder. After film deposition, the vacuum chamber was vented by introducing a N_2 gas evaporated from liquid nitrogen. The film thickness was measured with a mechanical stylus profilometer (DEKTAK IID) having a nominal resolution of 0.5 nm. The film thickness was determined as the average value of at least seven profilometry measurements obtained from different surface regions of each sample.

B. Microstructural analysis

The sputtered carbon films were characterized by X-ray photoelectron spectroscopy (XPS) using a Kratos Analytical XPS/XAES spectrometer with a monochromatic X-ray source of Al Kα (1486.6 eV). The spectrometer was operated at a constant pass energy of 20 eV, with an analyzer resolution equal to 2% of the pass energy. A 0.1 eV energy step was used to acquire the XPS spectra of the C 1s and N 1s transitions. The approximately 2 mm x 0.5 mm spot illuminated by the Al Kα monochromator yielded an area resolution for the XPS analyzer of ~1 mm^2. To minimize uncertainties in the binding energy measurements, all samples of each group were mounted on a copper block using conductive silver colloid paint. The pressure in the XPS analyzing vacuum chamber was better than 5 x 10^{-9} Torr. The samples were not subjected to Ar^+ bombardment for sputter cleaning before the XPS analysis.

Information about the film compositions was extracted from characteristic core level peaks using published sensitivity factors. Deconvolution of the C 1s and N 1s peaks (after using Shirley background subtraction) and fitting with Gaussian distributions at characteristic binding energies were performed according to the method described by Sherwood.[24] The full-width-half-magnitude values of the Gaussian profiles corresponding to the C 1s and N 1s peaks are between 1.8 eV and 2.3 eV. Each Gaussian profile of the C 1s and N 1s peaks was associated with a film constituent at a certain chemical state using characteristic binding energies at different environments.[3,5,25-27] Atomic percentages of each constituent were determined from the calculated areas under the corresponding Gaussian profiles.

C. Nanoindentation testing

The surface roughness and nanomechanical properties of the sputtered carbon films were studied with a surface force microprobe apparatus (Hysitron Inc.) interfaced with an atomic force microscope (Nanoscope II, Digital Instruments). For surface roughness measurement, a sharp

diamond tip of radius less than 100 nm was used to scan 1 μm x 1 μm film surface areas at a contact force of 0.5 μN. To evaluate the nanomechanical properties of the films, a pyramidal diamond tip with an included angle of 90° and a nominal radius of ~20 nm was used to perform indentations on the coated silicon samples. The shape function of the diamond tip was determined by indenting a standard ultrasmooth fused quartz sample of nanohardness H equal to 10 GPa. The indentation contact depth h_c in the calibration experiments with the fuzed quartz sample was in the range of 1-25 nm, and the measured in-plane elastic modulus $E/(1-\nu^2)$ of fuzed quartz was ~73.3 GPa. The tip-shape calibration procedure was repeated frequently to monitor any changes of the tip shape due to possible wear during testing. The indentation load P was applied incrementally using an isosceles triangular force profile with a peak value of 20 μN and total load/unload time equal to 6 s. The indentation contact depths obtained with this technique were in the range of 2-10 nm. The projected contact area A_c was determined from a tip-shape polynomial function of the contact depth at maximum indentation load. The latter may differ from the set peak force value due to the mechanical response of the indented films. (Normally, the softer the material the greater the deviation from the set value of the peak normal load.) The nanohardness and reduced elastic modulus E_r of the films were determined from the corresponding force versus indentation depth curves. In this study, nanohardness is defined as the maximum indentation load divided by the corresponding projected contact area. According to Nix,[28] the reduced elastic modulus is given by,

$$\frac{1}{E_r} = \frac{1-\nu_i^2}{E_i} + \frac{1-\nu_s^2}{E_s} \tag{1}$$

where E_i, E_s and ν_i, ν_s are the elastic modulus and Poisson's ratio of the indenter and the substrate materials, respectively. The elastic modulus and Poisson’s ratio of the diamond indenter, quoted

by the manufacturer, are 1140 GPa and 0.07, respectively. The reduced elastic modulus was calculated from the force-indentation depth curve using the relationship,

$$E_r = \frac{S}{2}\sqrt{\frac{\boldsymbol{p}}{A_c}} \tag{2}$$

where S is the elastic stiffness, defined as the slope of the indentation curve at the beginning of unloading (dP/dh). Hence, the in-plane elastic moduli of the films were easily determined from Eqs. (1) and (2) and the known properties of the diamond tip. At least five indentations were performed at different locations on each film surface. For statistical analysis, the nanohardness and elastic modulus data were assumed to follow normal distributions.

III. RESULTS AND DISCUSSION

A. Film growth kinetics and chemical compositions

The thickness t and rms roughness of the RF sputtered carbon films were found to be in the ranges of 10-35 nm and 0.18-0.22 nm, respectively, i.e. the produced film surface topographies were similar to that of the silicon substrate. Since the deposition time was fixed at 5 min, the average film growth rates at different N_2 partial pressures were between 2 and 7 nm/min.

Before considering the effects of deposition conditions on the chemical composition, surface roughness, thickness, microstructure, and nanomechanical properties of the sputtered films, it is instructive to consider first the kinetics of film deposition. Martino et al.[9] argued that while the mechanical and physical properties of sputtered carbon thin films synthesized at different chamber conditions using various gas mixtures are affected by the deposition kinetics, they are essentially independent of the resulting film composition. Although knowledge of the film composition is not sufficient to explain the mechanical properties, it may yield important insight into the kinetics of film deposition. Figures 1(a) and 1(b) show the dependence of the nitrogen and argon contents of the films on the volume percentage of N_2 in the sputtering gas mixture. As

expected, the amount of nitrogen in the film increases significantly with the N_2 volume percentage, conversely to the argon content. The small amount of nitrogen in the films deposited at zero N_2 partial pressure (samples A and E in Table I) is attributed to the partial saturation of the carbon dangling bonds on the film surfaces by the N_2 gas used to vent the chamber after the film deposition. There are different reasons for the incorporation of nitrogen and argon in the carbon films. Since a bias voltage of -200 V was applied to the substrate during deposition, the presence of argon and nitrogen in the film compositions may be attributed to Ar and N ion bombardment and reactions between N and C atoms during film growth.

The nitrogen and argon contents depend on their respective ion concentrations in the plasma, especially in the vicinity of the substrate surface, and their sticking probabilities at the growing film surface. The elemental ion concentrations depend on the RF power (since for a fixed power the plasma density in the discharge affects the target voltage), the transport characteristics of the gas mixture and the plasma, and the type of the sputtering system. Schwan et al.[29] used magnetron sputtering to increase the plasma density which promoted the incorporation of a relatively large amount of Ar in the sputtered a-C films. The plasma ion density in the discharge is also affected by the flow rate of the sputtering gas. Since the working pressure in the present experiments was fixed (3 mTorr), a higher pumping speed was used to increase the mass flow rate. This might have led to the loss of more electrons and ions to the chamber space and walls, especially in the absence of a magnetron confinement. The sticking probabilities of adatoms are functions of the reactivity of N and Ar atoms with C atoms and the intensity of energetic ion bombardment. Thus, in view of the relatively low kinetic energy (~200 eV), only small amounts of argon ions were implanted in the films, as shown in Fig. 1(b) and Table II. For all other deposition conditions fixed, the amount of argon in the films reflects the Ar^+ concentration in the plasma and is, therefore, indicative of the intensity of argon ions bombarding the substrate surface.

Conversely, the nitrogen content in the carbon films is mostly determined by the sticking probability of N atoms adsorbing on the growing film surface, which depends on the material system, kinetic energy of precursors, and energetic ion bombardment.

The target bias voltage determines the kinetic energy of ions impinging the target surface and depends on the plasma environment. As shown in Table I, the magnitude of the self-biased target voltage during RF sputtering increases with the N_2 partial pressure, revealing the existence of differences in the transport characteristics of the argon and nitrogen plasmas. For reactive RF magnetron sputtering in the presence of a pure nitrogen plasma, Kaltofen et al.[10] reported that the dominant process gas ions are N^+ and N_2^+. Since the masses of N^+ and N_2^+ are both much smaller than that of Ar^+, their mobility is relatively greater. Consequently, from the ion mass perspective and for fixed ion density, the self-biased target voltage in a nitrogen plasma environment should be lower than that in an argon plasma environment. However, Table I shows that the magnitude of the target bias voltage increases with the N_2 partial pressure. This can be explained by considering the role of other important parameters, such as mean free path, lifetime of metastable ions, and ionization degree of the plasma. Since the mean free path and lifetime of N^+ and N_2^+ are both shorter than those of Ar^+,[23] the possibility of recombination in the nitrogen plasma is greater than that in the argon plasma. Hence, for fixed control process parameters (e.g. RF power and chamber pressure), the ionization degree of the nitrogen plasma is less than that of the argon plasma and, hence, the ion density in the nitrogen plasma is lower. Therefore, the dependence of the self-biased target voltage on the N_2 content in the gas mixture can be explained by considering the aforementioned simultaneous effects. Since the self-biased target voltage during deposition changes from -1500 V to -1750 V with increasing amount of N_2 in the sputtering gas (Table I) and the potential of the bulk plasma is about +10 V with respect to the chamber walls, the kinetic energy of Ar and N ions bombarding the target surface increases from 1500 eV to 1750 eV. Thus,

the argon and nitrogen ion kinetic energies for sputtering material from the target surface were in the range of 1500-1750 eV, while for sputtering material from the growing film surface they were ~200 eV.

Film deposition comprises sputtering of film material from the target surface, transport of this material through the target-substrate space, and film growth on the substrate surface.[22,23] Consequently, the film growth rate depends on the sputtering rate of the target material (controlled by the sputtering yield and current density of ions bombarding the target surface), the geometrical configuration and scattering effect (affected by the mean free path of the precursors in the plasma environment), and the sticking probability of precursors on the growing film surface. Hence, film growth is strongly affected by the sputtering yield $\boldsymbol{x}$, defined as the number of atoms (or molecules) ejected from the bombarded surface per incident ion.

The sputtering yield is a function of the masses of incident ions and target atoms m_i and m_t, respectively, and the kinetic energy E of incident ions,[30,31] which depends mainly on the electrical fields resulting from the bias voltages occurring on the target and substrate surfaces. Since the density of sputtered-off target atoms is strongly affected by the energy transferred to the target surface,[32] the sputtering yield depends on the energy dissipated into the target surface, determined by the nuclear stopping power of the material system, which depends on the masses of incident ions and target atoms and the kinetic energy of impinging ions. In the kinetic energy range for physical sputtering, the nuclear stopping is the dominant mechanism of energy transfer by particle collision. The sputtering yield of target material can be determined by considering the cascade regime where a bombarding ion transfers energy to a chain of target atoms, which, in turn, transfer energy to other atoms in the solid by additional collisions. Only a few atoms can acquire sufficient energy from these collisions to escape from the surface. Experiments and simulations have shown that the critical kinetic energy for atom extraction from an ion bombarded surface is

typically 1 keV.[23,30-34] For ion kinetic energies less than 1 keV, the sputtering yield $\boldsymbol{x}$ depends on the energy transfer and is given by[32]

$$\boldsymbol{x} = \frac{3\boldsymbol{a}}{4\boldsymbol{p}^2} \frac{4m_i m_t}{(m_i + m_t)} \frac{E}{U_0} \tag{3}$$

where U_o is the surface binding energy of the sputtered material and $\boldsymbol{a}$ is a monotonic function of m_t/m_i, increasing from 0.17 to 1.4 as m_t/m_i increases from 0.1 to 10. For ion kinetic energies greater than 1 keV, the input energy is dissipated within a larger volume of target material, so that the energy dissipated in the surface layers remains virtually constant over a broad energy range. Therefore, the sputtering yield for bombarding energies above 1 keV is relatively constant, virtually independent of the bombarding ion energy E and the target atom density, and can be expressed as[32,33]

$$\boldsymbol{x} \propto \frac{m_i}{m_i + m_t} \frac{1}{U_0} \tag{4}$$

Since the ion kinetic energy for sputtering target material is between 1500 eV and 1750 eV, Eq. (4) indicates that the light N^+ and N_2^+ produce a lower sputtering yield than the heavy Ar^+. Conversely to the sputtering yield of the target material, the kinetic energy of ions bombarding the growing film surface is only ~200 eV, and Eq. (3) shows that the sputtering yield for N^+ and N_2^+ is greater than that for Ar^+. However, the simultaneous adsorption of the reactive N^+ and N_2^+ on both the film surface and the target surface reduces the apparent sputtering yields. It may be therefore interpreted that, for fixed ion kinetic energy, Ar^+ sputtering of the target and film surfaces is more pronounced.

In view of the substrate biasing in the present experiments, both argon and nitrogen ions sputtered off carbon material from the target surface and also weakly bonded adatoms on the growing film surface. Film growth depends on the numbers of both arriving and etched away film-

forming atoms.[22] The increase of the target voltage with the N_2 partial pressure (Table I) can be attributed to the different plasma transport characteristics resulting from variations in the gas mixture composition.[32] From Eq. (4) and for a target bias voltage between -1500 V and -1750 V, it follows that any changes in the sputtering yields of argon and nitrogen ions bombarding the graphite target can be neglected as insignificantly small.[33] For reactive gas of pure N_2, the exposed surface area of the graphite target subjected to energetic ion bombardment decreases due to the adsorption of nitrogen. This decreases the sputtering rate of carbon material from the target surface. In a pure Ar atmosphere, the sputtering rates of the target and film surfaces are high, whereas for a sputtering gas mixture containing ~90 vol% N_2 both rates decrease appreciably. Due to the competing film growth processes, the film growth rate attains a maximum at some intermediate value of the N_2 content. Hence, for a total mass flow rate of 20 sccm, Fig. 1(c) shows that the thicker films are produced when the sputtering gas mixture contains ~10 vol% N_2. At lower mass flow rates the film growth rate increases due to the higher ion density in the plasma produced at a fixed working pressure.

Figure 2 shows the variation of the global N/C ratio in the sputtered films with the N_2 vol% in the sputtering gas mixture. The N/C ratio increases rapidly in the range of 0-30 N_2 vol%, approaching a value of ~0.32 as the nitrogen content increases above 30 vol%. The results shown in Figs. 1 and 2 indicate that the mass flow rate of the sputtering gas affects the film growth rate, whereas the effect on the film compositions is marginal.

The presence of oxygen in the films (Table II) can be attributed to residual oxygen from the chamber walls and oxygen from the exposure to the atmosphere. The time of exposure to the air of the samples from the second and third sets was much shorter than that of the samples of the first set. The amount of oxygen incorporated in the films during deposition depends on the cleanness of the vacuum chamber, determined by the base pressure and the purity of the

sputtering gas. In view of the 99.999% purity of the Ar and N_2 gases used in the present study, it may be interpreted that the main sources of oxygen were the residual gas in the vacuum system and oxygen from the sample exposure to the atmosphere. This is also supported by the trend for the oxygen content to decrease with decreasing base pressure (Table II).

B. Microstructure and phase composition

Figure 3 shows typical C 1s and N 1s XPS spectra of the carbon films deposited at a N_2 partial pressure of 2.58 mTorr (sample D). Inelastic background subtraction and Gaussian profile fitting were applied to the spectra. The spectra show that both peaks comprise several features of varying binding energy levels corresponding to different bonding states of C and N atoms. Similar to all sputtered films of this study, there are six and five distinguishable features in the C 1s and N 1s spectra, respectively. The line positions and atomic percentages of these features for samples A-D are listed in Table III. Conversely to the study of Marton et al.,[3] the presence of amorphous carbon-carbon bonding is revealed by the carbon peaks at binding energies of ~284.4 eV and ~285.4 eV (denoted as C 1s (1) and C 1s (2) in Table III) corresponding to sp^2- and sp^3-coordinated carbon bonding states. The sp^2 and sp^3 contents in the amorphous phase can be estimated by using the deconvolution method of the C 1s XPS spectra proposed by Jackson et al.[26] and Diaz et al.[27] Marton et al.[3] ignored the carbon peak at ~284.5 eV as originating from adventitious carbon. However, this cannot explain the C 1s (1) and C 1s (2) peaks in the XPS spectra of the films produced in a nitrogen-free plasma atmosphere (e.g. samples A and E).

According to simulation results of Souto et al.,[25] the peak at binding energy of 398.2 eV is due to N atoms bonded to sp^3-coordinated C in a configuration resembling that of ***b***-Si_3N_4, whereas the peak at binding energy of 400.5 eV is attributed to substitutional N atoms in an sp^2 graphite-like configuration. Based on identifications for most other peaks similar to those in

previous studies of CN_x films,[3,5,25] it may be interpreted that the produced films contain two phases: a ***b***-C_3N_4-like phase with N atoms bonded to sp^3-hybridized C atoms, and a graphite-like phase with N atoms bonded to sp^2-hybridized C atoms. Marton et al.[3] reported that the binding energies of C^1 and N^1 in the ***b***-C_3N_4-like phase are equal to ~287.7 eV and ~398.5 eV, while those of C^2 and N^2 in the graphite-like phase are ~286.1 eV and ~400 eV, respectively. Therefore, the two carbon peaks at ~286.2 eV and ~287.5 eV in the C 1s spectrum (denoted as C 1s (3) and C1s (4) in Table III and C^2 and C^1 in Table IV) correspond to sp^2- and sp^3-hybridization bonding structures and are associated with the two different binding states of C atoms bonded to N atoms. The carbon peaks at ~289.3 eV and ~291.1 eV (denoted as C 1s (5) and C 1s (6) in Table III) are indicative of the binding states of C with O and C with both O and N, respectively. The two nitrogen peaks at ~400.2 eV and ~398 eV in the N 1s spectra (denoted as N 1s (2) and N 1s (1) in Table III and N^2 and N^1 in Table IV) are identified as the binding states of N atoms with sp^2- and sp^3-hybridized C atoms, respectively. The peak at ~399 eV in the N 1s spectra (denoted as N 1s (5) in Table III) is due to small amounts of N_2 gas physisorbed at the carbon film surfaces. The remaining two peaks at ~402 eV and ~404.5 eV (denoted as N 1s (3) and N 1s (4) in Table III) indicate the existence of N-N and N-O bonding, respectively.

The shape of the N 1s XPS spectrum of the a-CN_x films deposited at room temperature, -200 V substrate bias voltage, and sputtering gas containing 86 vol% N_2 (i.e. sample D) is almost the same as those of the CN_x films deposited by reactive magnetron sputtering on silicon substrates at 400 ^oC or 500 ^oC, zero substrate bias, and pure N_2 sputtering gas at 2.5 mTorr.[4,5] This suggests that the effect of energetic ion bombardment on the resulting bonding states is similar to that of raising the substrate temperature. Weakly bonded atoms can be easily removed either by bombarding the surface of the growing film with energetic ions or by substrate heating. Increasing the surface temperature may enhance the breakage of the weaker C-N bonds, thus

reducing the film nitrogen content. However, increasing the substrate temperature may also promote residual stress relaxation leading to structure ordering and softening, as evidenced from the experimental results of Yang et al.[7]

Based on the identified peaks and data given in Table III, the concentration and composition of each constituent in the carbon films were calculated after applying standard correction factors on the XPS measurements and results are listed in Table IV. Figure 4 shows that while the contents of both carbon nitride phases increase with the N_2 partial pressure, the content of the a-C matrix decreases. In addition, both compositions of the two phases, $[N^1]/[C^1]$ and $[N^2]/[C^2]$, are affected significantly by variations in the N_2 partial pressure. As the N_2 partial pressure increases from 0 to 2.7 mTorr (i.e. N_2 content increases from zero to 90 vol%), the N/C stoichiometric ratio in the ***b***-C_3N_4-like and graphite-like phases increases correspondingly from 0.06 to 1.09 and from 0.06 to 1.21 (Table IV), while the overall N/C ratio increases from 0.01 to ~0.32 (Table II and Fig. 2). These results indicate that less Ar^+ bombardment at ~200 eV promotes the incorporation of nitrogen into the forming film. Since the main carbon bonds in the a-C matrix are sp^2 and sp^3, corresponding to core level binding energies of ~284.4 eV and ~285.5 eV, respectively (Table III), the sp^3 content in the a-C matrix can be obtained from the two Gaussian fits at C 1s (1) and C 1s (2) in the C 1s XPS spectra, as shown in Table IV.

Although the sp^3 carbon contents of the a-C matrix are significantly different from those of the films deposited at different gas flow rates, Fig. 5(a) shows that the sp^2 and sp^3 carbon bonding fractions in the a-C matrix are relatively insensitive to variations in the amount of N_2 in the sputtering gas, as evidenced from the data for the sp^3 content in the a-C matrix given in Table IV and plotted in Fig. 5(a). Figures 5(b) and 5(c) show the dependence of the total sp^2 and sp^3 carbon contents of the carbon films on the N_2 vol% in the sputtering gas mixture. The total sp^3 carbon content is the sum of the sp^3 carbon contents of the a-C matrix and the ***b***-C_3N_4-like phase, and the

total sp^2carbon content is the sum of the sp^2carbon contents of the a-C matrix and the graphite-like phase. The total sp^2carbon content decreases with increasing the N_2 percentage in the gas mixture for both gas flow rates. The carbon films deposited at a gas flow rate of 20 sccm possess higher sp^3 contents (lower sp^2 contents) than the films deposited at total gas flow rates in the range of 8-13 sccm. For a fixed working pressure and substrate bias, increasing the gas flow rate decreases the ion density in the plasma and, in turn, the intensity of ion bombardment on the substrate surface. The results shown in Fig. 5 suggest that increasing the intensity of energetic ion bombardment promotes the formation of films possessing higher sp^2 carbon contents. Thus, while the compositions of the sputtered a-CN_x films depend predominantly on the N_2 partial pressure during deposition, the film microstructure is also affected by the total mass flow rate of the sputtering gas, which influences the ion bombardment intensity during film growth by changing the ion density in the discharge.

The amount of reactive gas in the chamber may be another reason for the different sp^3 carbon contents of the films deposited at a fixed working pressure. At a higher total mass flow rate, more reactive gas (N_2) is introduced into the chamber at a given time, which may lead to an abundance of nitrogen adsorption on the growing film surface. While most of the weakly-adsorbed nitrogen will be sputtered off due to the energetic ion bombardment, the temporary adsorption of nitrogen on the growing film surface may be beneficial to the increase of the sp^3 carbon bonding.

C. Nanomechanical properties

Figure 6 shows representative force versus indentation depth curves of sputtered carbon films. The remarkable differences between the loading and unloading portions of the indentation curves suggest that the films possess significantly different elastic-plastic material properties. The

almost identical loading and unloading patterns of the indentation curve shown in Fig. **6**(a) indicate that the deformation of the film deposited in the presence of a pure Ar plasma (sample A) is essentially elastic. A comparison of Figs. 6(b)-6(d) shows that the slopes of the loading and unloading portions of the indentation curves decrease and the force hysteresis area increases with increasing the amount of N_2 in the sputtering gas. These trends reveal that the film stiffness and resistance to plastic deformation decrease with increasing nitrogen content. For example, the residual indentation depth on the surface of the film deposited at 3.5 vol% N_2 (sample B) is ~ 2 nm (Fig. **6**(b)), while that on the film deposited at 86 vol% N_2 (sample D) is ~ 7 nm (Fig. 6(d)), despite the lower peak load in the latter indentation.

Results for the surface roughness, nanohardness, and in-plane elastic modulus are shown in Table V and Fig. 7. The nanohardness and in-plane elastic modulus of the Si(100) substrate are 12.77 ± 0.47 GPa and 143.43 ± 15.38 GPa, respectively. Table V shows that the surface roughness is marginally affected by changes in the process parameters and film growth rate; however, the effect on the nanomechanical properties of the films is significant. In particular, Fig. 7 reveals that both the film nanohardness and the in-plane elastic modulus decrease remarkably with increasing the nitrogen content in the sputtering gas mixture, despite the relatively small variations in the sp^3 and sp^2 carbon contents, shown in Figs. 5(b) and 5(c), respectively. This indicates that the material properties cannot be interpreted solely based on the magnitude of the sp^3/sp^2 ratio. For instance, the film obtained with a nitrogen-free sputtering gas (sample A) is much harder and stiffer than the film deposited at 86 vol% N_2 (sample D). In addition, the ratio of the hardness to the in-plane elastic modulus decreases from 0.23 to 0.13 with increasing the N_2 content. This ratio is regarded as a measure of the material resistance to plastic deformation; the higher the ratio, the higher the material resistance to plastic flow. The value of this ratio for other common hard materials such as sapphire, soda lime glass, tungsten, quartz, and diamond films is

0.06, 0.07, 0.08, 0.12, and 0.1, respectively.[35] Since the produced a-CN_x films exhibit relatively high elastic stiffness and hardness, they are promising candidate materials for protective overcoats. In addition, Fig. 7 shows that the film nanohardness and stiffness decrease with increasing the gas flow rate. This is again attributed to the lower ion density produced at higher gas flow rates that decreases the intensity of energetic ion bombardment on the growing film surface.

The trends shown in Fig. 7 can be attributed to the concomitant effects of less energetic ion bombardment on the growing film surface and the incorporation of soft phases in the a-C matrix. Energetic ion bombardment promotes film densification, development of compressive residual stresses, and etching of weakly bonded atoms on the growing film surface, thus increasing the average atomic bond strength in the film. Although increasing the N_2 partial pressure increases the density of N^+ and N_2^+ bombarding the film surface, it also reduces the density of bombarding Ar^+. Even though the kinetic energies of bombarding ions are the same, the heavier Ar^+ can sputter etch weakly bonded atoms much more effectively than the lighter N^+ and N_2^+ and, thus, the percentage of weak bonds increases with the N_2 partial pressure. In addition, Ar^+ bombardment is more effective in densifying the growing film and introducing compressive residual stresses than the N^+ and N_2^+ bombardment. The increasing shift of the C 1s (1) and C 1s (2) binding energies in the a-C matrix of the a-CN_x films (Table III) supports the view that the residual compressive stress relaxes as the Ar^+ bombardment decreases. It may be, therefore, argued that the main reasons for the lower nanohardness of the a-CN_x films deposited at a higher N_2 partial pressure are the relatively higher percentage of weak bonds and lower compressive residual stress resulting from the reduced Ar^+ bombardment.

For the ideal case of perfect crystallinity and appropriate N/C stoichiometry, ***b***–C_3N_4 is expected to exhibit a high hardness comparable to that of diamond. The nanohardness of the ***b***-

C_3N_4-like phase with $[N^1]/[C^1]$ ratio between 0.28 and 1.09 (Table IV) is unknown. Alternatively, the graphite-like phase is believed to be a relatively soft material, unless a fullerene-like microstructure of buckled sp^2-hybridized CN_x with a hardness of ~60 GPa and a high elastic recovery[21] can form due to the incorporation of relatively small amounts of nitrogen (~20 at%) under certain suitable conditions (e.g. gas mixture composition, substrate temperature, and substrate bias voltage).[5] In view of the above analysis, the decrease of the nanohardness and in-plane elastic modulus of the a-CN_x films with increasing N_2 partial pressure in the sputtering gas mixture can be mainly attributed to softening of the a-C matrix due to the reduced Ar^+ bombardment and the incorporation of larger amounts of soft phases (e.g. graphite-like phase).

IV. CONCLUSIONS

In this study, a-CN_x films with thickness in the range of 10-35 nm were deposited on Si(100) substrates by reactive RF sputtering using a pure graphite target and a sputtering gas mixture consisting of Ar and N_2 at a total working pressure fixed at 3 mTorr. XPS analysis and surface force microprobe microscopy were used to study the dependence of the surface roughness, composition, microstructure, and nanomechanical properties of a-CN_x films on the N_2 partial pressure and to explain the underlying mechanisms. In light of the presented results and discussion, the following main conclusions can be drawn.

(1) The film nitrogen content increases and the argon content decreases with increasing the volume percentage of N_2 in the sputtering gas mixture. For a total mass flow rate of 20 sccm, the maximum film growth rate occurs at ~10 vol% N_2 due to the effects of competing film growth processes. Under optimum deposition conditions, the effect of the N_2 partial pressure in the sputtering gas mixture on the film surface roughness is secondary.

(2) The a-CN_x films consist of an a-C matrix containing two phases: a ***b***-C_3N_4-like phase with N atoms bonded to sp^3-hybridized C atoms and a graphite-like phase with N atoms bonded to sp^2-hybridized C atoms.

(3) The N/C stoichiometric atomic ratios in the ***b***-C_3N_4-like and graphite-like phases differ significantly from the global N/C atomic ratio. Increasing the N_2 partial pressure from zero to 2.58 mTorr (i.e. increasing the N_2 in the sputtering gas from zero to 86 vol%), increases the N/C ratios in the ***b***-C_3N_4-like and graphite-like phases from 0.06 to 1.09 and from 0.06 to 1.21, respectively, while the global N/C atomic ratio increases from 0.01 to 0.32.

(4) The nanohardness and in-plane elastic modulus of the sputtered a-CN_x films decrease with increasing amount of N_2 in the sputtering gas mixture during film deposition. This is attributed to the less pronounced effect of energetic ion bombardment on the growing film surface, responsible for the removal of weakly bonded atoms, and the simultaneous incorporation of soft phases (e.g. graphite-like) in the a-C matrix of the sputtered carbon films.

(5) While the total mass flow rate of the sputtering gas mixture does not affect the film composition, it affects the growth rate, microstructure, and nanomechanical properties of the a-CN_x films.

ACKNOWLEDGMENTS

This research was supported by the Surface Engineering and Tribology Program of the National Science Foundation under Grant No. CMS-9734907 and the Computer Mechanics Laboratory at the University of California at Berkeley. The authors are grateful to Dr. S. W. Yeh from Chevron Chemical Co., Richmond, California, for obtaining the XPS spectra.

References

[1]A. Y. Liu and M. L. Cohen, Science **245**, 841 (1989).

[2]A. Y. Liu and M. L. Cohen, Phys. Rev. B **41**, 10727 (1990).

[3]D. Marton, K. J. Boyd, A. H. Al-Bayati, S. S. Todorov, and J. W. Rabalais, Phys. Rev. Lett. **73**, 118 (1994).

[4]W. T. Zheng , H. Sjostrom, I. Ivanov, K. Z. Xing, E. Broitman, W. R. Salaneck, J. E. Greene, and J.-E. Sundgren, J. Vac. Sci. and Technol. A **14**, 2696 (1996).

[5]H. Sjostrom, L. Hultman, J.-E. Sundgren, S. V. Hainsworth, T. F. Page, and G. S. A. M. Theunussen, J. Vac. Sci. and Technol. A **14**, 56 (1996).

[6]B. Zhang, B. Wei, D. Sullivan, and H. Gotts, IEEE Trans. Magn. **33**, 3109 (1997).

[7]M. M. Yang, J. Chao, and M. Russak, IEEE Trans. Magn. **33**, 3145 (1997).

[8]N. Axen, G. A. Botton, R. E. Somekh, and I. M. Hutchings, Diamond Related Mater. **5**, 163 (1996).

[9]C. De Martino, F. Demichelis, G. Fusco, and A. Tagliaferro, Diamond Related Mater. **5**, 461 (1996).

[10]R. Kaltofen, T. Sebald, and G. Weise, Thin Solid Films **290-291**, 112 (1996).

[11]N. Laidani, A. Miotello, A. Glisenti, C. Bottani, and J. Perriere, J. Phys. Condens Matter **9**, 1743 (1997).

[12]D. Lee, H. Lee, and B. Park, J. Mater. Res. **12**, 2057 (1997).

[13]H. Xin, C. Lin, S. Zhu, S. Zou, Nuc. Instrum. Meth. Phys. Res. **B103**, 309 (1995).

[14]A. Komar, H. L. Chan and N. B. Dahotre, J. Mater. Eng. Perf. **6**, 583 (1997).

[15]X. Zhao, C. W. Ong, Y. C. Tsang, and Y. W. Wong, Appl. Phys. Lett. **66**, 2652 (1995).

[16]J. Narayan, J. Reddy, N. Biunno, and S. M. Kanetkar, Mater. Sci. Eng. B **26**, 49 (1994).

[17]A. Khurshudov, K. Kato, and D. Sawada, Tribol. Lett. **2**, 13 (1996).

[18]X. He, L. Shu, W. Li, and H. Li, J. Mater. Res. **12**, 1595 (1997).

[19]Y. Taki, T. Kitagawa, and O. Takai, Thin Solid Films **304**, 183 (1997).

[20]M. Zhang and Y. Nakayama, J. Appl. Phys. **82**, 4912 (1997).

[21]H. Sjostrom, S. Stafstrom, M. Boman, and J.-E. Sundgren, Phys. Rev. Lett. **75**, 1336 (1995).

[22]W. Lu and K. Komvopoulos, J. Appl. Phys., (1998) (to be submitted).

[23]M. Konuma, *Film Deposition by Plasma Techniques*, Springer-Verlag, (1992).

[24]P. Sherwood, *Practical Surface Analysis by Auger and X-ray Photoelectron Spectroscopy*, edited by D. Briggs and P. Seah, John Wiley, New York, (1983).

[25]S. Souto, M. Pickholz, M. C. dos Santos, and F. Alvarez, Phys. Rev. B **57**, 2536 (1998).

[26]S. T. Jackson, R. G. Nuzzo, Appl. Surf. Sci. **90**, 195 (1995).

[27]J. Diaz, G. Paolicelli, S. Ferrer, and F. Comin, Phys. Rev. B **54**, 8064 (1996).

[28]W. D. Nix, Metall. Trans. A **20**, 2217 (1989).

[29]J. Schwan, S. Ulrich, H. Roth, and H. Ehrhardt, J. Appl. Phys. **79**, 1416 (1996).

[30]J. E. Mahan and A. Vantomme, J. Vac. Sci. and Technol. A **15**, 1976 (1997).

[31]P. Sigmund, Phys. Rev. **184**, 383 (1969).

[32]B. Chapman, *Glow Discharge Processes: Sputtering and Etching*, John Wiley, New York, (1980).

[33]M. A. Lieberman and A. J. Lichtenberg, *Principles of Plasma Discharges and Materials Processing*, John Wiley, New York, (1994).

[34]M. Ohring, *The Materials Science of Thin Films*, Academic Press, (1992).

[35]J. Martin-Gil, F. J. Martin-Gil, M. Sarikaya, M. Qian, M. Jose-Yacaman, and A. Rubio, J. Appl. Phys. **81**, 2555 (1997).

Table I. Deposition conditions of reactive RF sputtering of carbon films

Sample	N_2 partial pressure (10^{-3} Torr)	N content (vol%)	N_2 flow rate (sccm)	Ar flow rate (sccm)	Target voltage (V)	Base pressure (10^{-6} Torr)
A	0	0	0	11.59	-1500	5.0
B	0.11	3.5	0.42	11.59	-1550	1.8
C	0.93	31	4.00	8.70	-1660	2.2
D	2.58	86	7.20	1.16	-1710	2.5
E	0	0	0	20	-1500	1.5
F	0.15	5	1	19	-1600	3.0
G	0.30	10	2	18	-1620	1.5
H	0.60	20	4	16	-1680	2.7
I	1.20	40	8	12	-1720	1.5
J	2.40	80	16	4	-1750	4.0

Table II. **Compositions of RF sputtered carbon films determined from XPS analysis**

Sample	C (at%)	N (at%)	Global N/C	Ar (at%)	O (at%)
A	89.85	0.94	0.010	1.95	6.95
B	87.53	4.70	0.054	1.53	6.09
C	74.79	17.93	0.240	0.76	6.36
D	70.44	22.78	0.323	0.05	6.36
E	94.80	0.48	0.005	1.55	3.14
F	87.62	7.02	0.080	1.45	3.89
G	84.09	10.61	0.126	1.42	3.87
H	80.56	14.20	0.176	0.95	4.25
I	75.88	19.46	0.256	0.56	4.07
J	72.36	23.74	0.328	0.07	3.83

Table III. **Binding energies (BE) of the Gaussian profiles and corresponding atomic percentages in XPS spectra of RF sputtered carbon films**

Feature	Sample							
	A		B		C		D	
	BE (eV)	at%	BE (eV)	at%	BE (eV)	at%	BE (eV)	at%
N 1s (1)	398.68	0.26	398.04	1.48	397.99	7.44	398.08	10.35
N 1s (2)	400.18	0.42	400.19	2.71	400.26	9.02	400.21	10.78
N 1s (3)	401.75	0.14	402.24	0.32	402.62	1.01	402.62	1.23
N 1s (4)	405.72	0.07	404.68	0.12	404.67	0.32	404.77	0.36
N 1s (5)	399.28	0.05	398.93	0.07	399.09	0.15	399.09	0.28
C 1s (1)	284.38	57.11	284.21	56.54	284.50	41.19	284.66	37.41
C 1s (2)	285.44	18.56	285.33	9.92	285.50	7.61	285.65	6.89
C 1s (3)	286.69	6.93	286.12	11.08	286.18	13.27	286.27	11.52
C 1s (4)	288.15	3.99	287.65	5.34	287.51	8.04	287.39	9.51
C 1s (5)	289.66	2.12	289.31	2.93	289.23	3.09	289.07	3.52
C 1s (6)	291.40	1.14	291.14	1.73	291.17	1.59	291.02	1.59

Table IV. **Concentration and composition of constituents in RF sputtered carbon films**

Sample	Film constituent					
	Amorphous Carbon (a-C)		***b***-C_3N_4-like Carbon Nitride N-C (sp^3)		Graphite-like Carbon Nitride N-C (sp^2)	
	a-C (at%)	sp^3 (%)	$[C^1]+[N^1]$ (at%)	$[N^1]/[C^1]$	$[C^2]+[N^2]$ (at%)	$[N^2]/[C^2]$
A	75.91	24.85	4.25	0.06	7.35	0.06
B	66.46	14.74	6.82	0.28	13.79	0.24
C	48.81	15.59	15.48	0.93	22.29	0.68
D	44.30	15.49	19.86	1.09	22.30	0.94
E	78.59	28.26	4.77	0.04	5.88	0.04
F	66.81	31.22	8.99	0.32	11.44	0.48
G	61.24	30.13	10.48	0.55	14.51	0.59
H	52.54	25.40	15.04	0.64	18.63	0.62
I	49.27	27.84	19.68	0.81	18.78	0.85
J	45.99	27.95	23.26	1.02	19.04	1.21

Table V. **Thickness, surface roughness, maximum contact depth, nanohardness, and in-plane elastic modulus of RF sputtered carbon films**

Sample	t (nm)	rms (nm)	h_c (nm)	H (GPa)	$E/(1 - \mathbf{n}^2)$ (GPa)	$H(1-\mathbf{n}^2)/E$
A	10	0.20	2.0-2.8	39.19 ±3.53	185.10 ±9.00	0.212
B	16	0.19	3.9-4.7	25.46 ±1.64	143.88 ±4.34	0.177
C	22	0.18	6.4-7.5	16.69 ±0.93	105.76 ±4.44	0.158
D	13	0.18	8.4-9.9	12.53 ±0.76	95.14 ±5.01	0.132
E	10	0.20	1.8-4.1	37.58 ±8.95	160.61 ±18.97	0.234
F	20	0.22	4.6-6.6	22.88 ±3.01	117.11 ±10.8	0.195
G	33	0.21	6.1-7.2	19.43 ±1.24	106.97 ±5.42	0.182
H	21	0.19	8.1-9.2	14.79 ±0.89	95.82 ±2.25	0.154
I	15	0.19	8.0-8.8	15.25 ±0.63	93.42 ±4.50	0.163
J	7	0.18	9.3-10.3	12.69 ±0.72	97.33 ±2.79	0.133

List of Figures

FIG. 1. Nitrogen and argon contents in the sputtered carbon films and film thickness versus volume percentage of N_2 in the sputtering gas mixture for different total gas flow rates. The standard deviation error bars in (a) and (b) are smaller than the size of data points (the maximum standard deviation value is 0.27 (Fig. 1(a))).

FIG. 2. Variation of the global N/C atomic ratio in the carbon films with the volume percentage of N_2 in the sputtering gas mixture for different total gas flow rates.

FIG. 3. Typical C 1s and N 1s XPS spectra of carbon films sputtered at N_2 partial pressure of 2.58 mTorr in a total pressure of 3 mTorr (sample D) with Gaussian distribution fits. The spectra were obtained after inelastic background subtraction.

FIG. 4. Content of constituent phases in the carbon films versus volume percentage of N_2 in the sputtering gas mixture.

FIG. 5. Variation of the contents of (a) a-C matrix, (b) total sp^3 bonding, and (c) total sp^2 bonding in the carbon films versus volume percentage of N_2 in the sputtering gas mixture for different total mass flow rates.

FIG. 6. Force versus indentation depth curves for N_2 partial pressures of (a) 0 mTorr (sample A), (b) 0.11 mTorr (sample B), (c) 0.93 mTorr (sample C), and (d) 2.58 mTorr (sample D).

FIG. 7. Variations of (a) film nanohardness and (b) in-plane elastic modulus with volume percentage of N_2 in the sputtering gas mixture for different total gas flow rates.

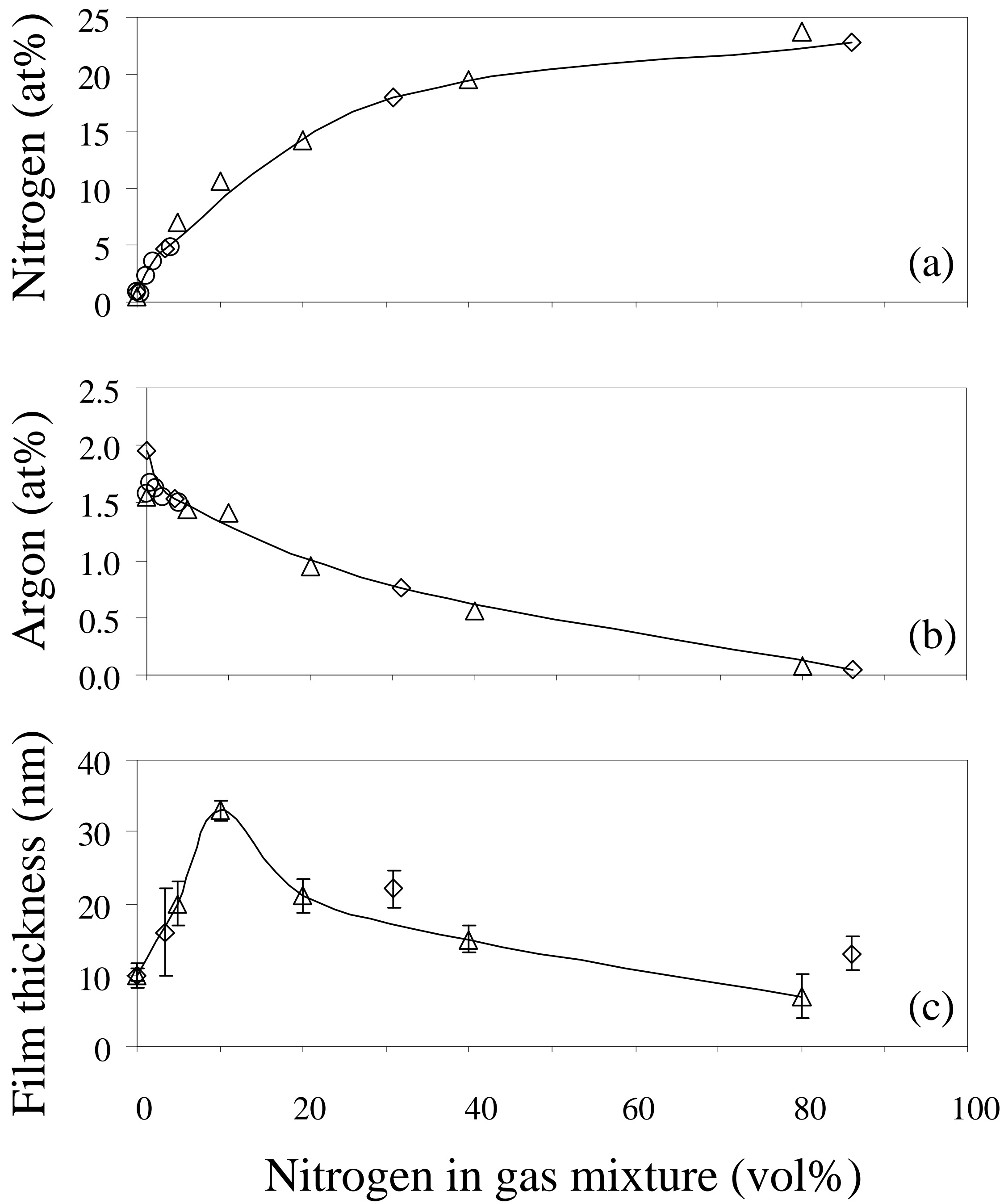

Figure 1

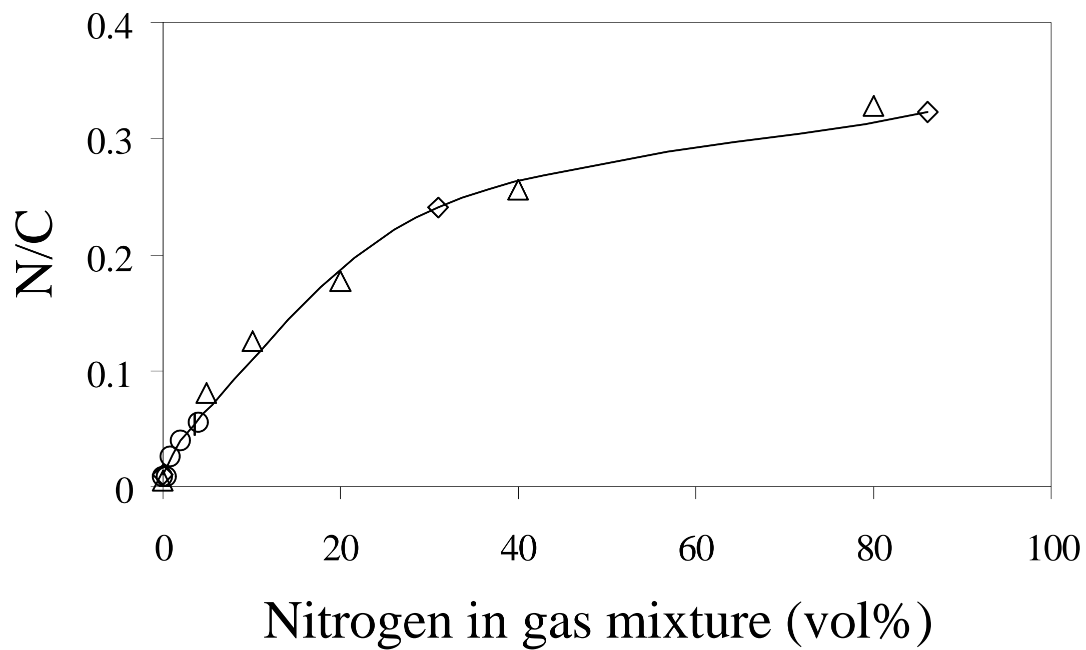

Figure 2

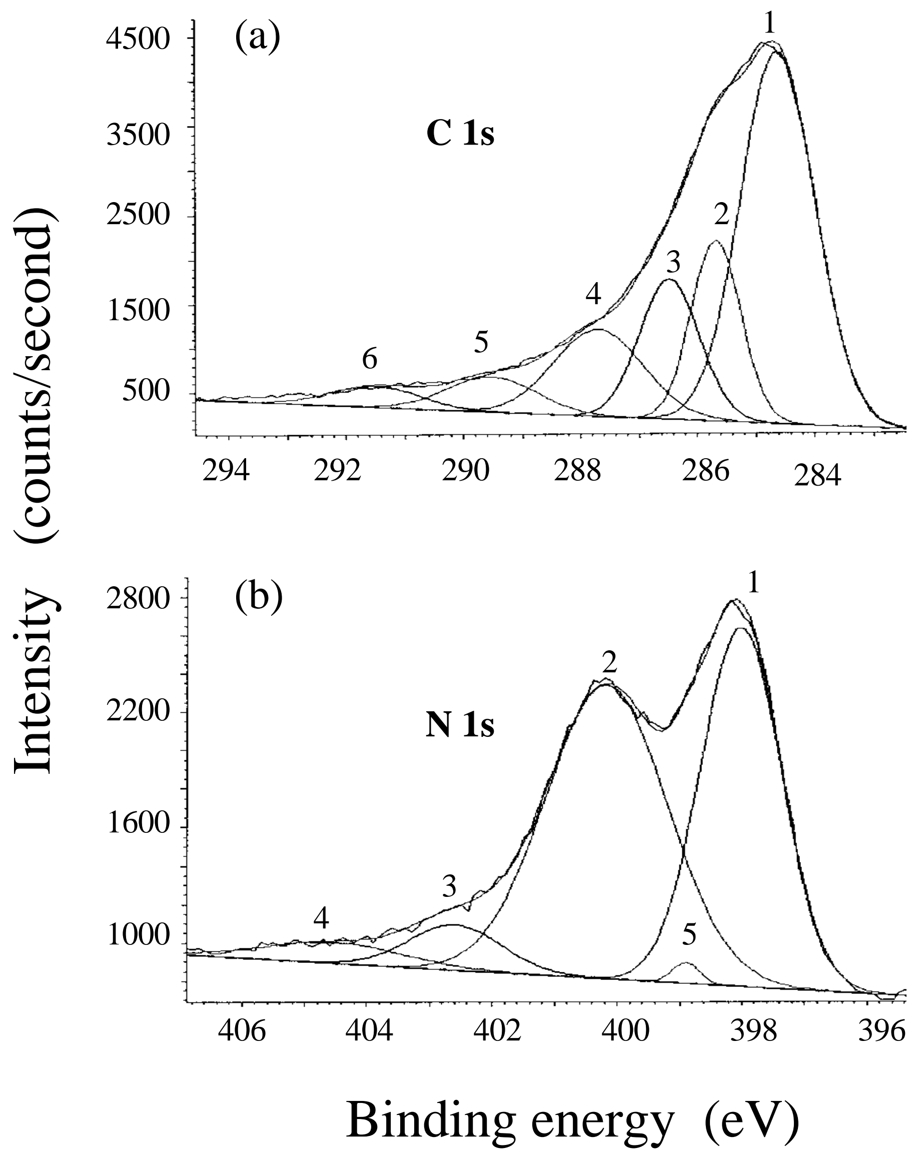

Figure 3

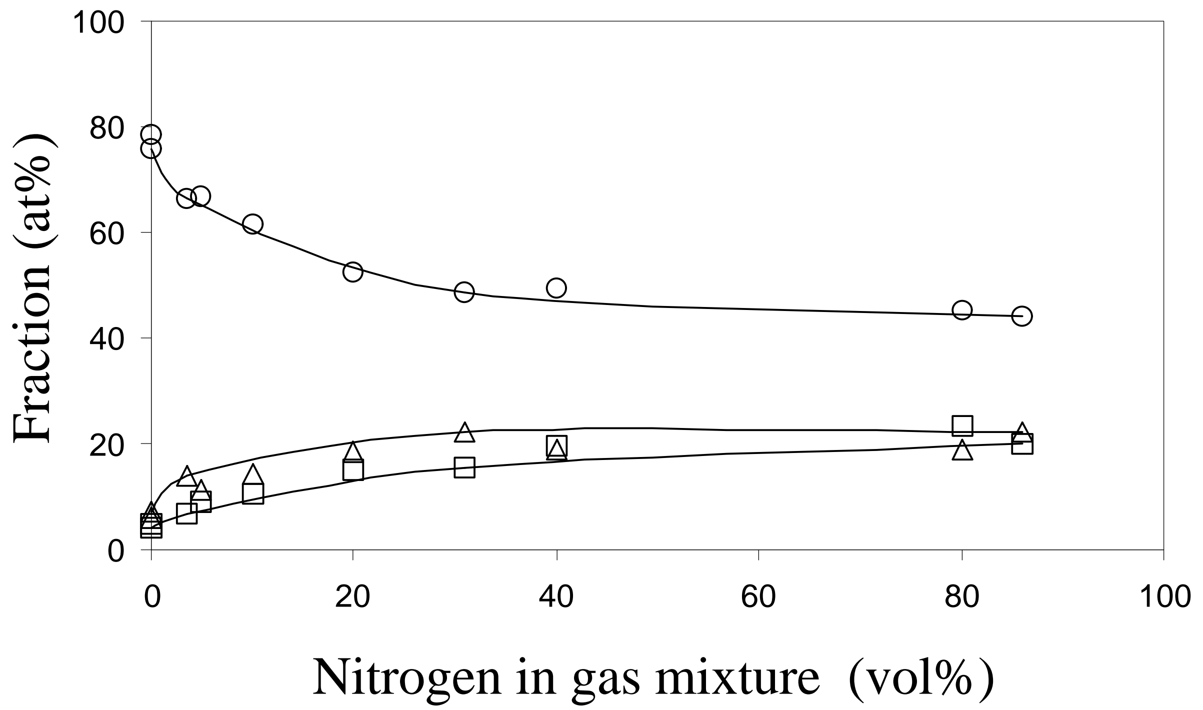

Figure 4

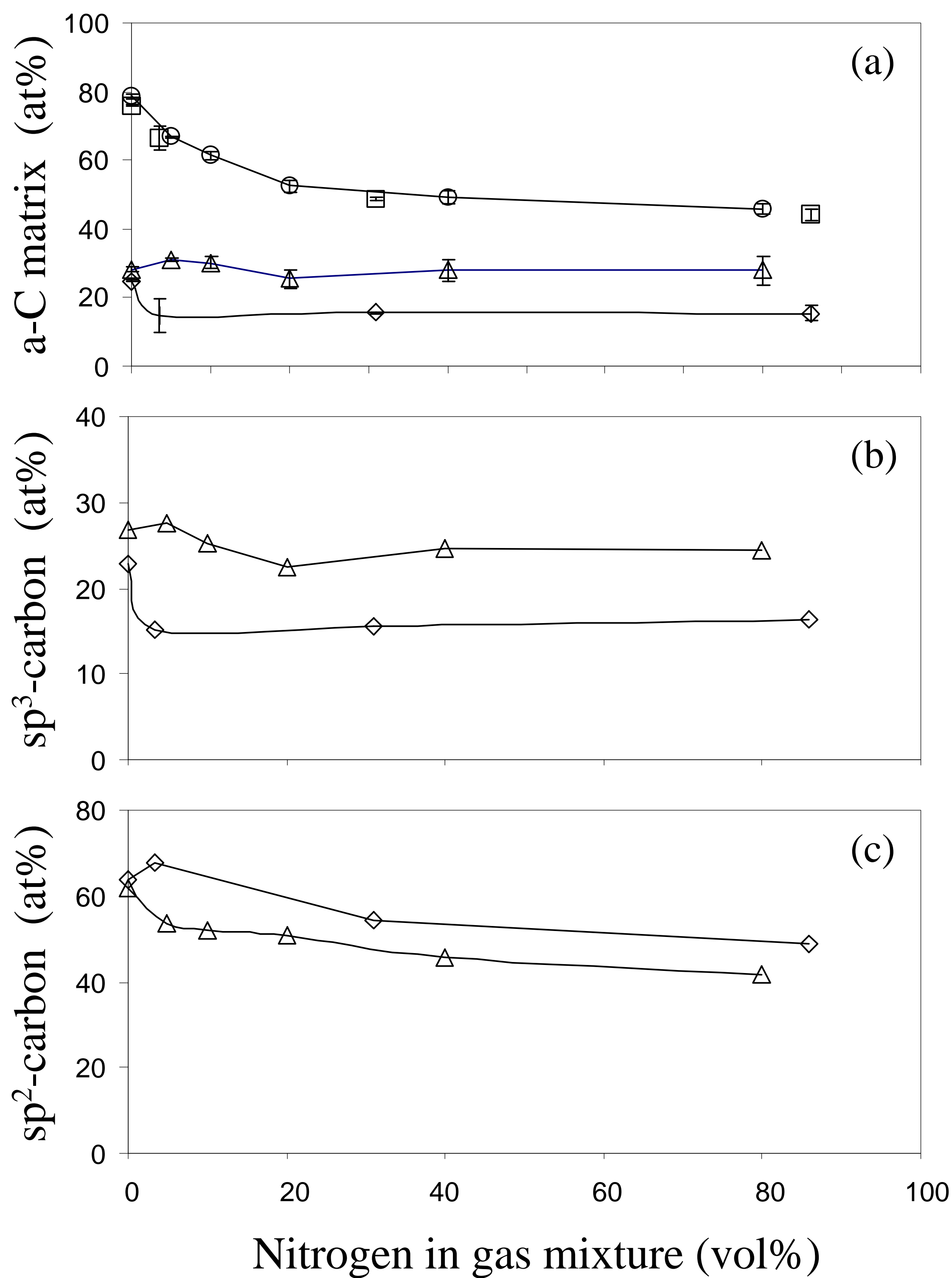

Figure 5

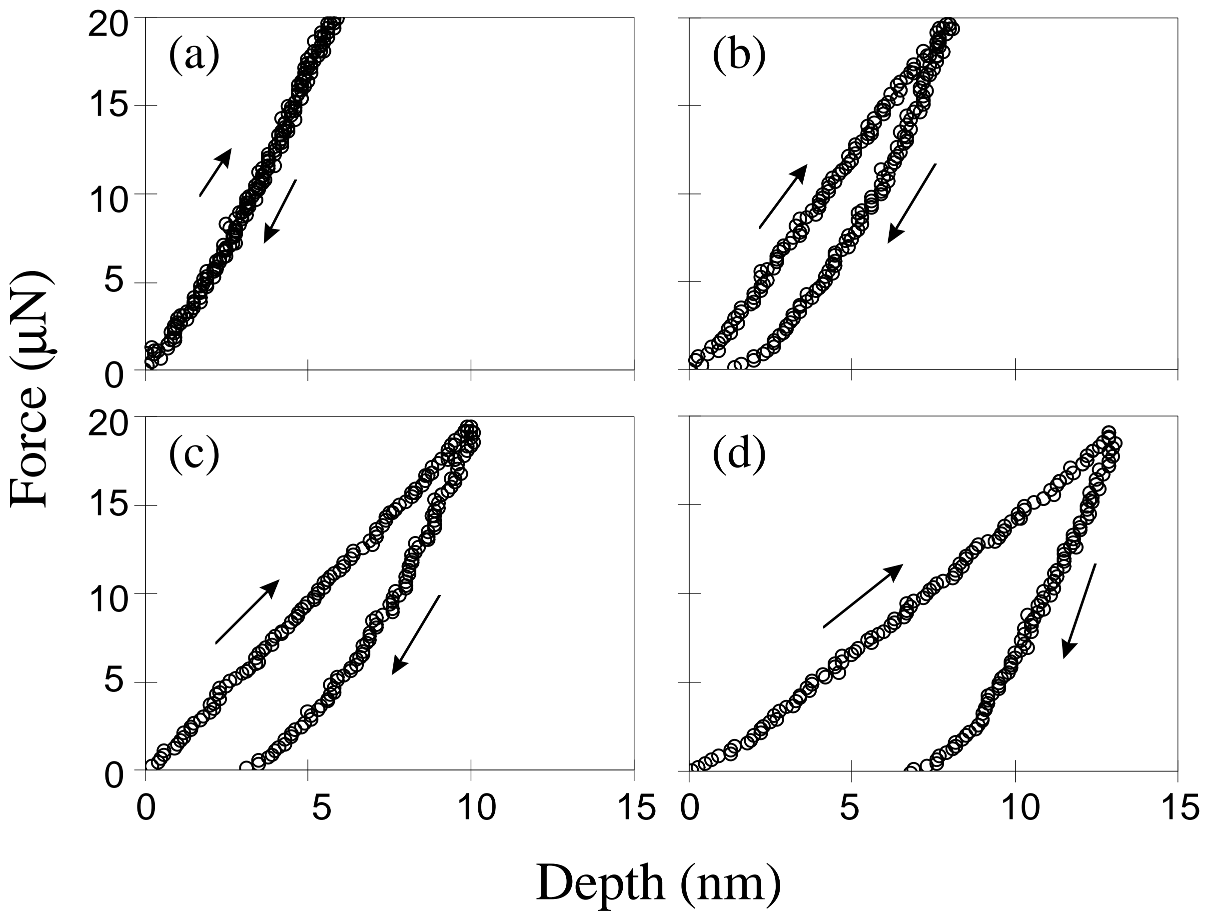

Figure 6

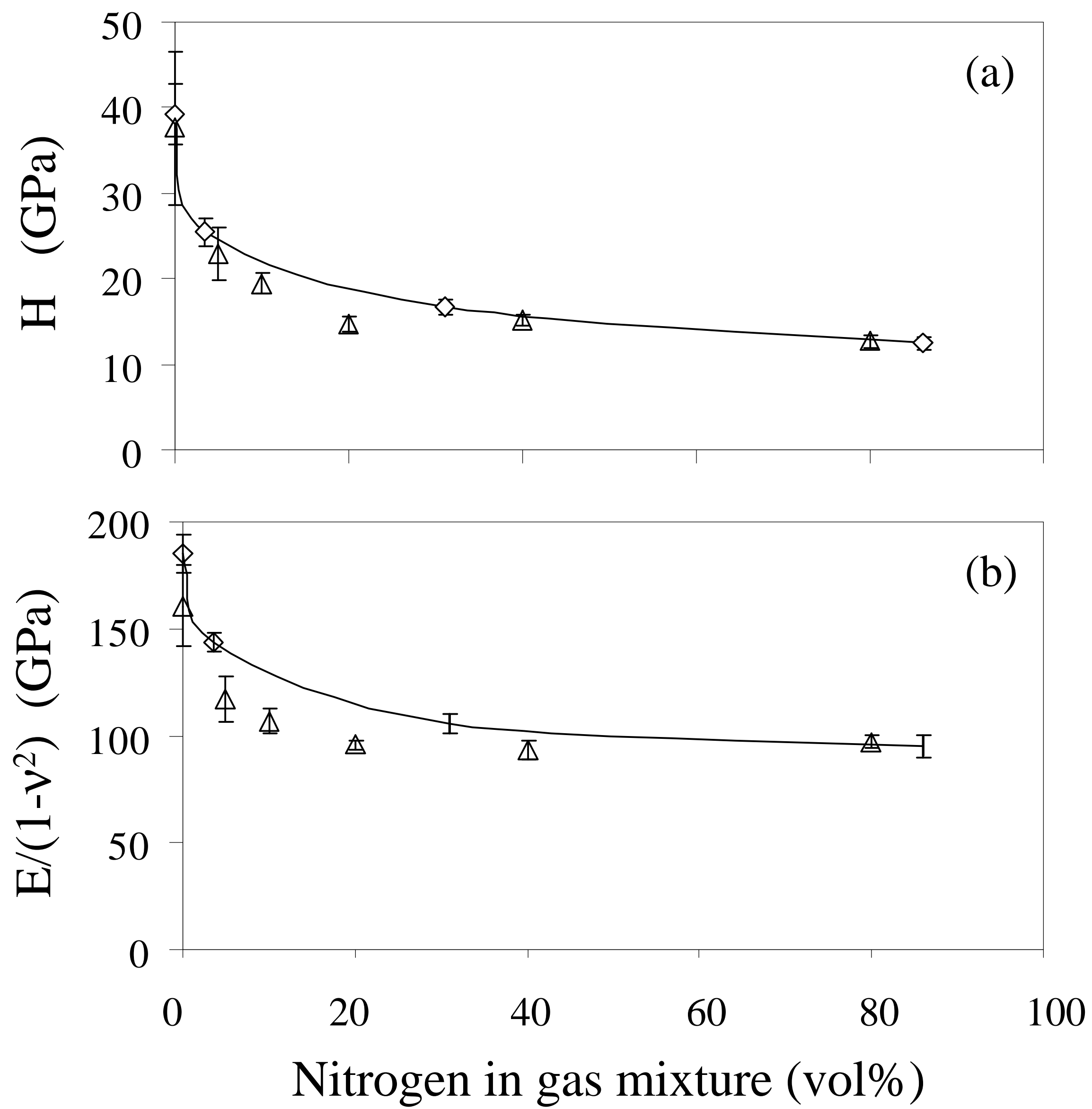

Figure 7